第 25卷第 6期　热能动力工程　Vol.25, No.6
2010年 11月　JOURNAL OF ENGINEERING FOR THERMAL ENERGY AND POWER　Nov., 2010

热力工程

文章编号: 1001－2060(2010)06－0621－06

流化床反应器内气固两相流动特性的研究

孙巧群[1], 高建民[2], 朱卫兵[1], 陆慧林[2]
(1. 哈尔滨工程大学 航天与建筑工程学院, 黑龙江 哈尔滨 150001;
2. 哈尔滨工业大学 能源科学与工程学院, 黑龙江 哈尔滨 150001)

摘　要: 基于颗粒动力学理论模拟颗粒相流动, 应用流体与颗粒两相流理论考虑两相相间作用, 建立了流化床核反应器内多相流流动的计算流体动力学模型, 数值模拟研究了流化床核反应器内的流体动力行为。计算结果表明, 应用 Gidaspow曳力模型得到的沿截面颗粒浓度分布与已有实验结果的分布趋势比较接近。在中心喷射区的中心处颗粒浓度较高。随着径向距离的增大, 逐渐降低到局部最小值后颗粒浓度逐渐上升。在环隙区域内颗粒浓度基本保持不变。分析了流体与颗粒间作用力、颗粒弹性恢复系数等对流化床核反应器内流体动力特性的影响。研究表明, 颗粒碰撞恢复系数越大, 流场内沿截面颗粒浓度分布变得越均匀。

关　键　词: 流化床核反应器; 两相流理论; 数值模拟
中图分类号: TK224.1　　文献标识码: A

引　言

流态化高温气冷堆具有非能动安全特性, 主要特征是采用流态化技术和高温气冷堆技术, 实现均匀的颗粒浓度、气相和燃料颗粒温度分布, 提高传热能力[1]。目前, 国际上已有关于流化床核反应器内气固两相运动特性研究的报道, 但发表的文献很少。其中采用流化床核反应器在床层被流化时, 床内存在大气泡和腾涌等流化恶化的现象[2], 这在很大程度上影响了反应器内核燃料颗粒的裂变反应率、堆内能量输出特性以及堆芯安全系数。而在国内关于带有倒锥体核反应器数值模拟领域的研究还未见报道。本研究采用的带有倒锥体流化床核反应器, 优点在于此种结构的流化床核反应器具有较高的对流换热系数和较大的热传导表面积以及较好的混合特性。由于在流化过程中气体和颗粒之间混合均匀, 提高了气固两相的接触效率, 从而增加了传热能力, 避免堆芯烧毁。

1　数学模型

流化床核反应器内流体动力学模型满足质量守恒、动量守恒和能量守恒原理。同时为了简化流化床核反应器内气体和颗粒流动计算, 假设: (1) 燃料颗粒为球形, 直径为常数; (2) 气体和燃料颗粒无反应, 流动为等温流动过程。对于等温气固两相流动过程, 连续性方程可以表示为 ($i=g$ 时为气体, $i=s$ 时为颗粒相):

$$\frac{\partial}{\partial t}(\rho_i\varepsilon_i)+\nabla\cdot(\rho_i\varepsilon_i u_i)=0 \tag{1}$$

式中: ρ_i— 相密度, kg/m³; ε_i— 相体积浓度; u_i— i 相速度, m/s。

气相动量守恒方程需要考虑气体与燃料球颗粒之间的相互作用, 可表示为:

$$\frac{\partial}{\partial t}(\varepsilon_g\rho_g u_g)+\nabla\cdot(\varepsilon_g\rho_g u_g u_g)=-\varepsilon_g\nabla p+\varepsilon_g\rho_g g+\beta(u_s-u_g)+\nabla\cdot\tau_g \tag{2}$$

式中: g—重力加速度, m/s; p—气相压力, Pa; β—气固两相间的曳力系数; μ_g—气相动力粘度, Pa·s; τ_g—气相应力张量:

$$\tau_g=\mu_g[\nabla u_g+(\nabla u_g)^T]-\frac{2}{3}\mu_g(\nabla\cdot u_g)I \tag{3}$$

同理, 颗粒相动量守恒方程除了需要考虑气体与颗粒之间的相互作用外, 还需要考虑颗粒相互碰撞产生的作用力:

$$\frac{\partial}{\partial t}(\varepsilon_s\rho_s u_s)+\nabla\cdot(\varepsilon_s\rho_s u_s u_s)=-\varepsilon_s\nabla p+\beta\times(u_g-u_s)+\nabla\cdot\tau_s+\varepsilon_s\rho_s g \tag{4}$$

式中: τ_s—固相应力张量, 由颗粒动理学方法固相应力可表示为[3~4]:

$$\tau_s=(-P_s+\lambda_s\nabla\cdot u_s)I+2\mu_s S\{[\nabla u_s+$$

收稿日期: 2010－03－06;　修订日期: 2010－06－12
基金项目: 国家自然科学基金资助项目 (50806019)
作者简介: 孙巧群 (1979－), 女, 浙江宁海人, 哈尔滨工程大学讲师.

$$(\nabla u_s)^T] - \frac{2}{3}(\nabla \cdot u_s) I\} \tag{5}$$

式中：p_s—颗粒相压力，Pa；λ_s—颗粒相表观粘度，μ_s—颗粒相动力粘度，Pa·s；p_s和μ_s由动力摩擦应力模型确定，它们分别为：

$$p_s=\varepsilon_s\rho_s[1+2(1+e)\varepsilon_s g_0]\Theta + Fr\frac{(\varepsilon_s-\varepsilon_{s,min})^n}{(\varepsilon_{s,max}-\varepsilon_s)^p} \tag{6}$$

$$\lambda_s=\frac{4}{3}\varepsilon_s\rho_s d_s g_0(1+e)\sqrt{\frac{\Theta}{\pi}} \tag{7}$$

$$\mu_s=\frac{4}{5}\varepsilon_s^2\rho_s d_s g_0(1+e)\sqrt{\frac{\Theta}{\pi}}+\frac{10\rho_s d_s\sqrt{\Theta\pi}}{96(1+e)g_0}\times\left[1+\frac{4}{5}\varepsilon_s(1+e)g_0\right]^2+Fr\frac{(\varepsilon_s-\varepsilon_{s,min})^n\sin\phi}{(\varepsilon_{s,max}-\varepsilon_s)^p\sqrt{I_{2D}}} \tag{8}$$

式中：$\varepsilon_{s,max}$、$\varepsilon_{s,min}$—填充颗粒浓度和临界颗粒浓度；Θ—颗粒温度，$(m/s)^2$，$\Theta=u'^2/3$，u'—颗粒的脉动速度，m/s；n、p和Fr—与颗粒材料物性有关的经验系数，对于玻璃珠，颗粒参数n、p、Fr分别为2.0、5.0和0.05[5]；ϕ—内摩擦角，(°)，ϕ为28.5°；I_{2D}—应变率张量第二不变偏量。

颗粒温度Θ可按固相脉动能量守恒方程确定：

$$\frac{3}{2}\left[\frac{\partial}{\partial t}(\varepsilon_s\rho_s\Theta)+\nabla\cdot(\varepsilon_s\rho_s\Theta u_s)\right]=(-\nabla p_s I+\tau_s):\nabla u_s+\nabla\cdot(k_s\nabla\Theta)-\gamma_s+\phi_s \tag{9}$$

式中：I—单位向量；k_s—颗粒相热传导系数；γ_s—颗粒脉动能耗散率；ϕ_s—气体与颗粒间脉动能交换，它们分别为：

$$k_s=\frac{75\rho_s d_s\sqrt{\pi\Theta}}{192(1+e)g_0}\left[1+\frac{6}{5}(1+e)g_0\varepsilon_s\right]^2+2\varepsilon_s^2\rho_s(1+e)\sqrt{\frac{\Theta}{\pi}} \tag{10}$$

$$\gamma_s=3(1-e^2)\varepsilon_s^2\rho_s g_0\Theta\left(\frac{4}{d_s}\sqrt{\frac{\Theta}{\pi}}-\nabla\cdot u_s\right) \tag{11}$$

$$\phi_s=-3\beta\Theta \tag{12}$$

式中：e—颗粒非弹性碰撞恢复系数；d_s—颗粒直径，m；g_0—颗粒径向分布函数：

$$g_0=\frac{3}{5}\left[1-\left(\frac{\varepsilon_s}{\varepsilon_{s,max}}\right)^{1/3}\right]^{-1} \tag{13}$$

由于颗粒的离散特性，对于颗粒群的受力进行理论分析非常困难；通常颗粒的滞止阻力较其它受力更为重要，对颗粒的运动起支配作用。在气固系统中，实验观测到由于邻近颗粒的存在，颗粒的阻力较单颗粒的阻力要大，因此在计算稠密气固两相流时需要考虑邻近颗粒的影响，即对阻力系数进行修正，将其与颗粒雷诺数以及颗粒体积分数进行关联。对阻力系数的修正主要来自实验的数据，其中阻力系数修正式为：

（1）基于Ergun方程的阻力公式适用于稠密的固定颗粒床：

$$F_D=\frac{V_s\beta}{1-\varepsilon_g}(u_g-u_s) \tag{14}$$

$$\beta=150\frac{\varepsilon_s^2\mu}{\varepsilon_g(\phi_s d_s)^2}+1.75\varepsilon_s\frac{\rho_g}{\phi_s d_s}|u_g-u_s| \tag{15}$$

（2）Wen & Yu的指数修正公式适用于较稀疏的两相流：

$$\beta=\frac{3}{4}C_D\frac{\varepsilon_s\rho_g|u_g-u_s|}{d_s}\varepsilon_g^{-2.65} \tag{16}$$

$$C_D=\begin{cases}\frac{24}{Re}(1+0.15Re^{0.687}) & Re\leqslant 1000\\ 0.44 & Re>1000\end{cases} \tag{17}$$

（3）Gidaspow模型[6]，在稀相区和密相区分别采用Wen & Yu公式以及Ergun方程：

$$\beta=\begin{cases}150\frac{\varepsilon_s^2\mu}{\varepsilon_g(\phi_s d_s)^2}+1.75\varepsilon_s\frac{\rho_g}{\phi_s d_s}|u_g-u_s| & \varepsilon_g\leqslant 0.8\\ \frac{3}{4}C_D\frac{\varepsilon_s\rho_g|u_g-u_s|}{d_s}\varepsilon_g^{-2.65} & \varepsilon_g>0.8\end{cases} \tag{18}$$

（4）Arastoopour修正式[7]：

$$\beta=\left[\frac{17.3}{Re}+0.336\right]\frac{\rho_g}{d_s}|u_g-u_s|\varepsilon_s\varepsilon_g^{-2.8} \tag{19}$$

（5）DiFelice修正式[8]：

$$f(\varepsilon_g)=\varepsilon_g^{\alpha} \tag{20}$$

$$\alpha=4.7-0.65\exp\left[-\frac{(1.5-\lg Re)^2}{2}\right] \tag{21}$$

（6）Syamlal-O'Brien阻力模型[9]：

$$\beta=\frac{3}{4}C_D\frac{\varepsilon_g\varepsilon_s\rho_g}{V_r^2 d_s}|u_g-u_s| \tag{22}$$

$$C_D=\left(0.63+4.8\sqrt{\frac{V_r}{Re}}\right)^2 \tag{23}$$

$$V_r=\frac{1}{2}\left[a-0.06Re+\sqrt{(0.06Re)^2+0.12Re(2b-a)+a^2}\right] \tag{24}$$

$$a=\varepsilon_g^{4.14} \tag{25}$$

$$b=\begin{cases}0.8\varepsilon_g^{1.28} & \varepsilon_c\leqslant 0.85\\ \varepsilon_g^{2.65} & \varepsilon_c>0.85\end{cases} \tag{26}$$

式中：Re—颗粒雷诺数，$Re=\frac{\varepsilon_g\rho_g d_s|u_g-u_s|}{\mu}$

2　模拟结果和分析

在气相入口处, 给定入口轴向气体速度 u_{in}, 径向速度为零; 在壁面处采用无滑移条件; 出口条件, 取充分发展的管流条件 $\frac{\partial\phi}{\partial x}=0$ ($\phi=u, v$)。近壁面处采用壁面函数处理方法。u方程: $\tau_{wall}=C_f\frac{1}{2}\varepsilon_g\rho_g u^2$; v方程: $\tau_{wall}=C_f\frac{1}{2}\varepsilon_g\rho_g v^2$。其中, $C_f=0.003$为摩擦系数。

对颗粒相, 取入口颗粒速度为零; 在壁面处颗粒为无滑移条件, $u_s=v_s=0$, 出口条件, 取充分发展的管流条件, $\frac{\partial\phi_s}{\partial r}=0$ ($\phi_s=\rho_s, u_s, v_s, \Theta$)。

采用带有倒锥体的流化床核反应器结构及反应器内流动如图 1所示, 反应堆堆芯内存储一定量的燃料球颗粒, 氦气作为冷却剂。气体由反应堆底部进入, 流过燃料球颗粒, 形成高温气体, 最后由反应器顶部送出。反应器的几何尺寸借鉴 Pain等人的流化床核反应器结构[1], 在模拟的反应器内假设流动为轴对称。Pain等人采用的冷却流体为氦气[1], 流化床核反应器的运行压力为 6 MPa, 模拟计算时的冷却氦气密度为 0.162 5 kg/m^3, 核燃料颗粒直径和颗粒密度分别为 25 mm和 1 920 kg/m^3。

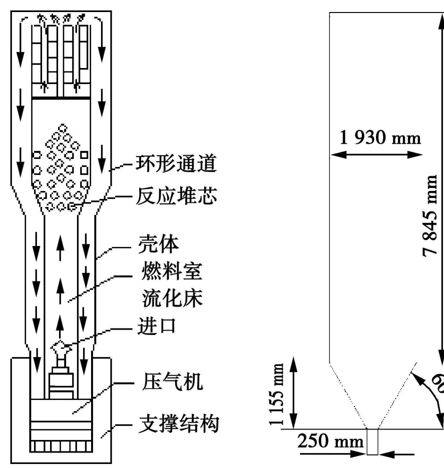

图 1　流化床核反应器堆芯结构

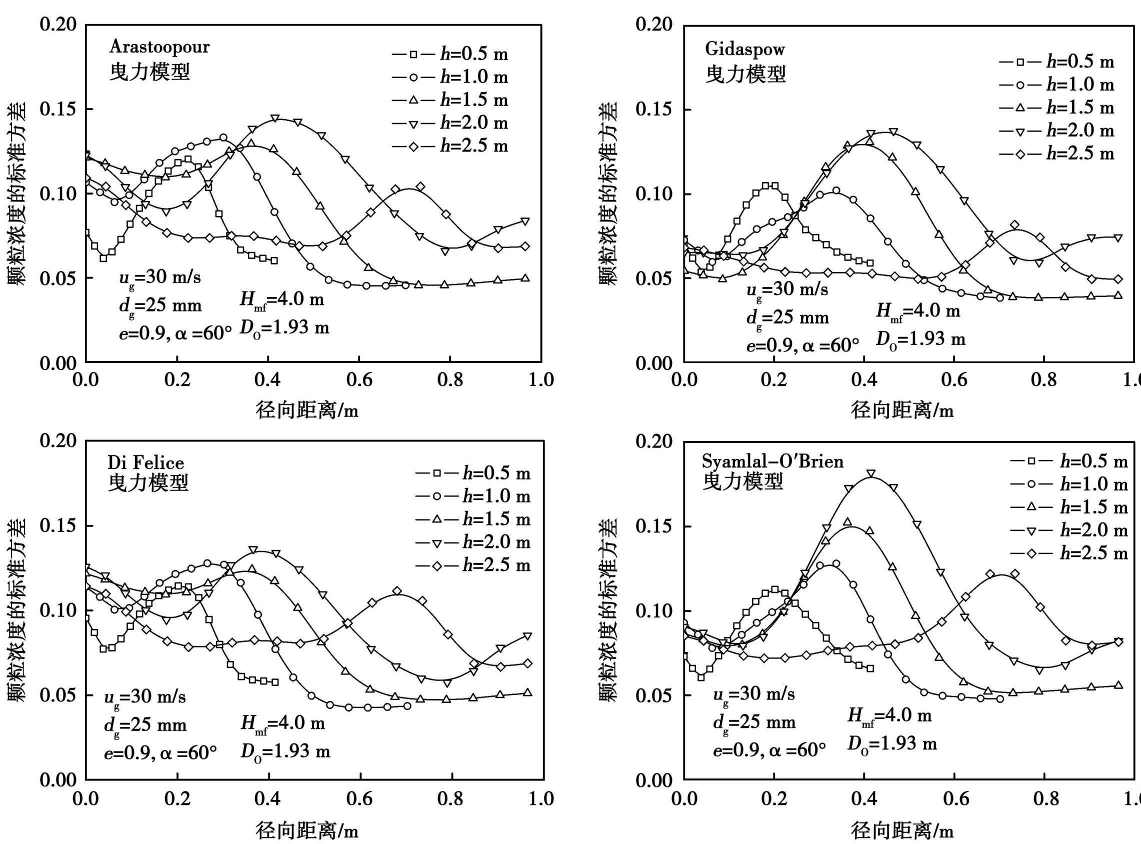

图 2　颗粒浓度标准方差的径向分布

图 2为入口射流速度 30 m/s时采用不同曳力模型床内颗粒浓度的标准方差分布。直观地可以用流场各部分的颗粒浓度 ε_s的标准方差 σ 来定量衡量计算域内颗粒分布的不均匀程度 (其中 $\sigma=$

$\sqrt{\sum_{i=1}^{N}(\varepsilon_i+\varepsilon_{av})^2/N}$，$\varepsilon_{av}$为平均颗粒浓度，N为计算样本数）。采用 Arastoopour模型、Syamlal-O'Brien模型以及 Di Felice模型进行模拟的结果表明，在喷泉高度位置以下，颗粒浓度的标准方差沿径向方向由中心向壁面先逐渐上升后降低，其中局部峰值的位置随着床层高度的增加逐渐向壁面方向移动。其中采用 Arastoopour模型和 Di Felice模型得到颗粒浓度标准方差在中心射流区内较大，这是由于在床层中产生了汽泡，从而导致了在中心射流和两侧环形区的界面处颗粒浓度的标准方差值也较大。采用 Syamlal-O'Brien模型计算时由于受到锥体影响较大，因此在中心射流区和环形区的界面处颗粒浓度方差值较高。从图中可以看出，采用 Gidaspow曳力模型得到的颗粒浓度标准方差要小于采用 Arastoopour模型、Syamlal-O' Brien模型以及 Di Felice模型得到的颗粒浓度标准方差值。

图 3表示入口射流速度 30 m/s采用不同曳力模型时反应器内颗粒浓度概率密度分布。模拟计算结果表明在经过约 10 s时间后流动进入稳定状态。取此时间后的计算结果，对反应器内空间进行统计，可以得到反应器内的浓度概率：$p(\varepsilon_s)=\sum_{t=t_0}^{t}\sum_{i=1}^{N}\frac{n_i}{N}$，其中 n_i为颗粒浓度在 ε_s至 $\varepsilon_s+\Delta\varepsilon_s$之间出现的次数，N为总统计数。显然，$\sum p(\varepsilon_i)=1.0$。针对不同曳力模型的模拟结果表明，颗粒浓度的概率分布出现了双峰分布的特征，分别是在低颗粒浓度区域和高颗粒浓度区域。研究结果表明，靠近高颗粒浓度的峰值贡献来自于两侧环形区内的稠密区颗粒流动，而靠近低颗粒浓度的峰值贡献来自于中心射流区域内的稀相区颗粒流动。两个峰值的分布取决于环形区和中心射流区的界面流动过程。结合瞬时颗粒浓度分布图可知，在中心射流区域内高速气体射流携带向上运动，此区域是低颗粒浓度区出现概率高的区域，形成了峰值。由于气体射流在向床面运动过程中不断与射流区进行动量交换，极大消耗了射流初始动量，直至到达最大床层膨胀高度时，由于气体射流速度的骤然降低，颗粒因重力作用沿两侧环形区内回流。因此在环形区内是出现高颗粒浓度区概率较高的区域。

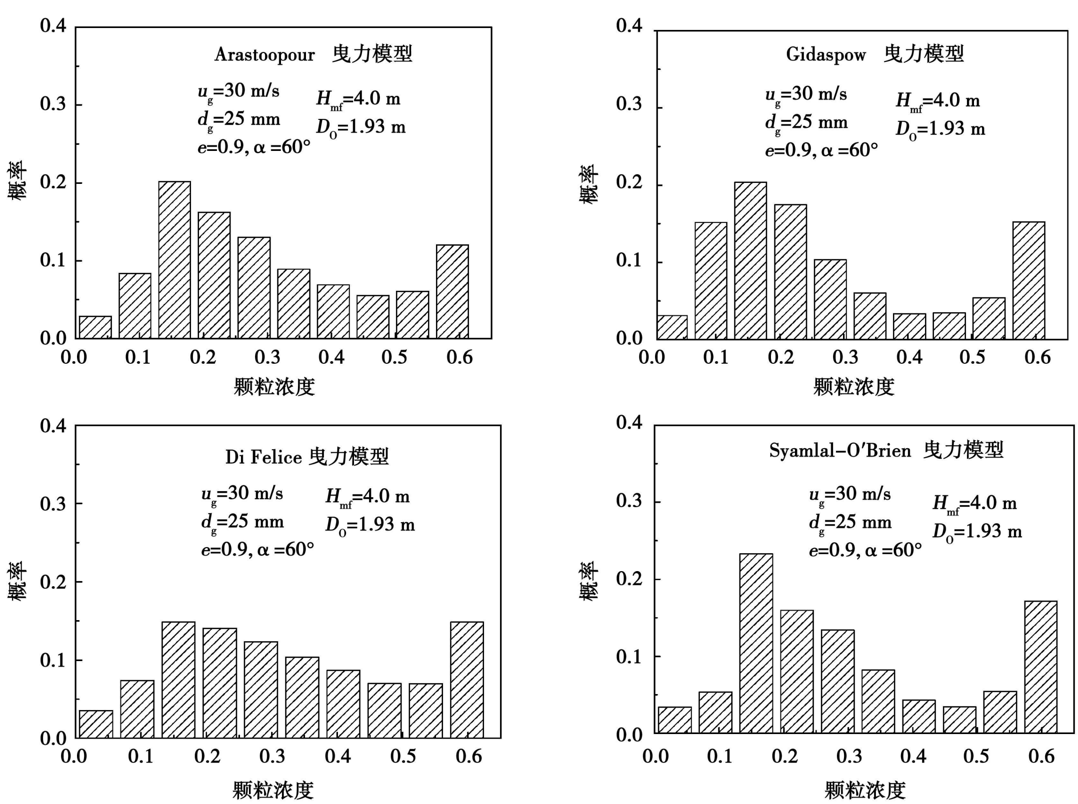

图 3 颗粒浓度的概率分布

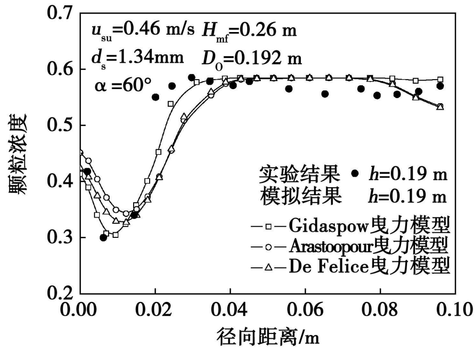

图 4　床内颗粒浓度的分布

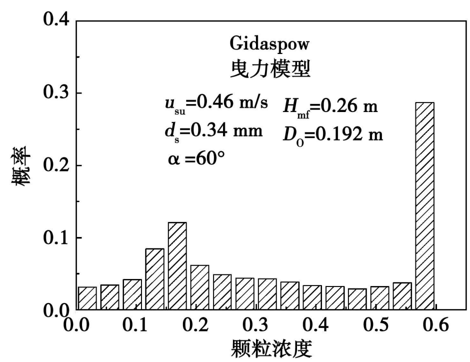

图 5　颗粒浓度的概率分布

3　模拟结果和实验结果的比较

迄今, 喷动床颗粒浓度测量数据十分有限, 大部分采用了对于稠相测量并不敏感的光纤技术。由于直径为 25 mm的 D类颗粒流化床实验结果尚未见, 因此采用李水清等实验条件结合本研究的理论模型进行预测。其中李水清等应用电容探针技术对喷动床颗粒浓度进行了测量[10]。实验装置为内径 192 mm、高 1 200 mm的圆柱体和锥角 60°、高 144 mm的圆锥体连接而成的喷动床, 入口直径为 25.72 mm。假设喷动床初始条件为临界流化状态。临界流化速度和流化状态空隙率根据 Ergun方程迭代计算得出。射流入口速度设定为给定值, 出口采用压力出口条件。

图 4和图 5分别表示表观气体速度为 0.460 m/s时喷动床内颗粒浓度分布和颗粒浓度的概率分布。由颗粒浓度沿径向方向分布图可知, 在中心喷射区处的颗粒浓度较高。随着径向距离的增大, 颗粒浓度逐渐降低到局部最小值后逐渐上升。在环隙区域内颗粒浓度基本保持不变。当采用 Gidaspow曳力模型得到的在床高 h=190 mm颗粒浓度沿径向方向分布与李水清等人采用电容探针技术得到的测量值趋势比较接近[10]。其中采用 Arastoopour和 DiFelice曳力模型得到的颗粒浓度分布与实验测量值误差较大。由图可知, 在中心射流区域内颗粒浓度大于测量值, 而在靠近壁面区域的颗粒浓度值要小于测量值。从颗粒浓度概率分布图可以看出, 颗粒浓度的概率分布分别在低颗粒浓度区域内出现概率较小的峰值和高颗粒浓度区域内概率较大的峰值。研究结果表明, 靠近低颗粒浓度区域的峰值主要是由中心射流区域内稀相区的颗粒流动引起的; 在高浓度区域的峰值是由两侧环形区内稠密区颗粒流动引起的。

4　颗粒弹性恢复系数的影响

图 6是入口射流速度 30 m/s弹性恢复系数分别为 e=0.8, e=0.9, e=0.95时床内颗粒浓度的概率分布。从图中可以看出, 当颗粒弹性恢复系数较小时, 在颗粒浓度为 0.6时, 存在较大的颗粒浓度概率分布峰值; 弹性恢复系数为 0.9时, 在颗粒浓度为 0.6则颗粒浓度概率峰值是逐渐降低的, 在低颗粒区域的颗粒浓度概率分布是逐渐增加的; 当弹性恢复系数增加到 0.95时, 在低颗粒区域的颗粒浓度概率分布出现了较大的峰值, 而在高颗粒浓度区域的颗粒浓度概率峰值逐渐消失, 研究结果表明, 流场内颗粒浓度分布趋于均匀。

5　结　论

采用流体与颗粒两相流理论考虑两相间作用, 对流化床核反应器内流体动力特性进行了数值模拟。

(1) 曳力是流化床核反应器内颗粒所受的主要加速力, 曳力模型的选择对反应器内颗粒浓度的分布有重要的影响。采用 Gidaspow曳力模型得到的颗粒浓度分布比较均匀; 使采用流态化技术的流化床核反应器内燃料颗粒浓度的分布变得均匀, 提高了核反应器的传热能力。

(2) 采用颗粒浓度的概率分布来描述流场内颗粒分布的整场特征, 研究发现增加颗粒碰撞恢复系数使得颗粒浓度概率分布在高浓度区的峰值逐渐降低, 引起流场内颗粒浓度分布变得均匀, 有利于提高核反应器的安全性。

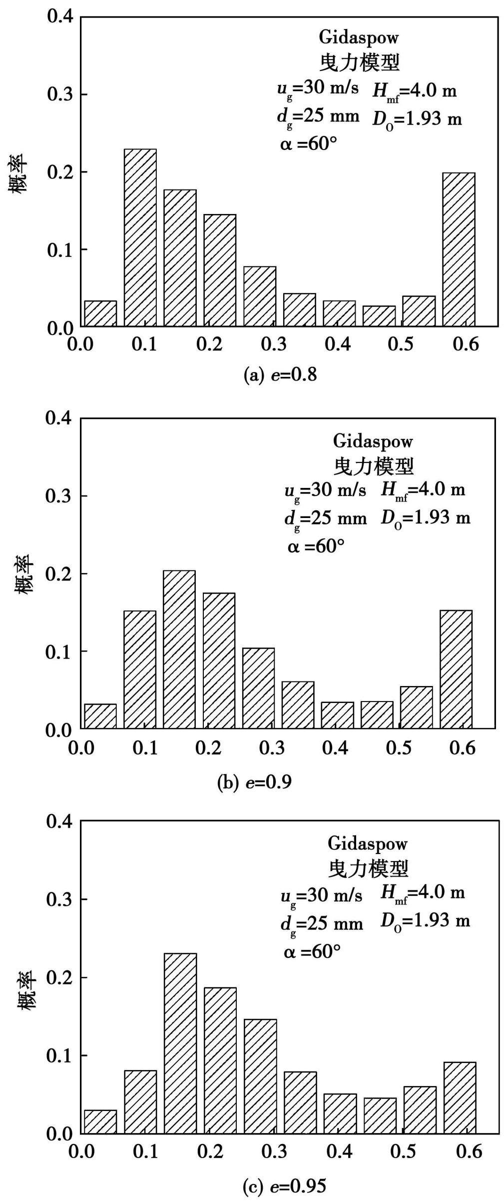

图 6 颗粒浓度的概率分布

参考文献:

[1] PAIN C C, GOMES J L M A, EATON M D. Space-dependent kinetics simulation of a gas-cooled fluidized bed nuclear reactor[J]. Nuclear Engineering and Design, 2002, 219: 225—245.

[2] PAIN C C, MANSOORZADEH S, DE OLIVEIRA C R E. A study of bubbling and slugging fluidized beds using the two-fluid granular temperature model[J]. International Journal of Multiphase Flow, 2001, 27: 527—551.

[3] LUN C K K, SAVAGE S B, JEFFREY D J, et al. Kinetic theory for granular flow: inelastic particles in coutte flow and slightly inelastic particles in a general flow field[J]. J Fluid Mech, 1984, 140: 223—256.

[4] CAMPELL C S. The stress tensor for simple shear flows of granular material[J]. J Fluid Mech, 1989, 203: 449—473.

[5] JOHNSON P C, NOTT P, JACKSON R. Frictional-collisional equations of motion for particulate flows and their application to chutes[J]. J Fluid Mech, 1990, 210: 501—535.

[6] DING J, GIDASPOW D. A bubbling fluidization model using kinetic theory granular flow[J]. J AIChE, 1990, 36(4): 523—538.

[7] ARASTOOPOUR H, PAKDEL P, ADEWUMI M. Hydrodynamic analysis of dilute gas-solids flow in a vertical pipe[J]. Powder Technology, 1990, 62(2): 163—170.

[8] DI FELICE R. The voidage function for fluid-particle interaction systems[J]. International Journal of Multiphase Flow, 1994, 20: 153—159.

[9] SYAMLAL M, O' BRIEN T J. Simulation of granular layer inversion in liquid fluidized beds[J]. Int J Multiphase Flow, 1988, 14(4): 473—481.

[10] 李水清, 姚 强, 赵香龙, 等. 喷动床内颗粒浓度的实验测量和理论模拟[J]. 工程热物理学报, 2005, 26(5): 871—874

(编辑 陈 滨)

致 读 者

随着科学技术的迅猛发展, 科研成果层出不穷, 大量的科技论文有待发表, 为了尽快解决压稿现象, 及时报道科研成果, 从 2011年起,《热能动力工程》杂志由原 112页增加到 128页, 每期定价由原 12元调整到 18元, 全年定价为 108元。

特此说明

——编辑部

With Fluent6.3 serving as a platform, a partial heat non-equilibrium model was adopted to numerically study the non-Darcian forced convection heat exchange in the vertical passages of a skeleton heat generation porous medium in a turbulent flow zone and its transition one. Three-dimensional N—S equation and standard k—ε turbulent flow model were used to depict the flow inside the porous medium. On this basis, the influence of the change in the pore effective Reynolds number Re (400< Re< 2000), surface heat flux density q (q=5 kW/m², 30 kW/m² and 90 kW/m²) and coolant inlet temperature T_{in} (T_{in}=20 ℃, 50 ℃ and 80 ℃) on the flow resistance and heat exchange characteristics was studied in detail. The research results show that at a low heat flux density, the change of surface heat flux density has a very small influence on the flow resistance and heat exchange coefficient. However, the diameter of the small balls exercises a significant influence on the heat exchange coefficient and such an influence will increase with an increase of Reynolds number. Moreover, the heat exchange coefficient will decrease with an increase of the coolant inlet temperature. Key words: skeleton heat generation, porous medium, numerical simulation

膜式全热换热器 EHD电场强化换热的实验研究 = Experimental Study of the EHD (Electrohydrodynamics)-based Electric Field Intensified Heat Exchange of a Membrane Type Full Heat Exchanger[刊，汉] / SUN Shu-hong, LU Yuan-wei, LU Guang-lin, et al (Education Ministry Key Laboratory on Heat Transfer Intensification and Process Energy Conservation, Beijing University of Technology, Beijing, China, Post Code: 100124) // Journal of Engineering for Thermal Energy & Power. — 2010, 25(6). —617~620

To enhance the heat exchange efficiency of a membrane type full heat exchanger, a high voltage electric field was applied to the heat exchanger. Under the same test conditions, the influence of the electric field applied from outside on the heat exchange effectiveness was analyzed by measuring both sensible and latent heat efficiency of the exchanger. On this basis, the heat exchange effectiveness of the exchanger was tested at various voltages of electric poles and different wind speeds. The test results show that the application of a high voltage electric field to the flow field of the heat exchanger can effectively enhance its sensible heat efficiency but insignificantly increase its latent heat efficiency. At a low wind speed, the intensified heat exchange effectiveness will be even more conspicuous. Key words: full heat exchanger, intensified heat exchange, electrohydrodynamics (EHD)

流化床反应器内气固两相流动特性的研究 = Investigation of the Gas-solid Two-phase Flow Characteristics Inside a Fluidized Bed Reactor[刊，汉] / SUN Qiao-qun, ZHU Wei-bing (College of Astronautics and Architectural Engineering, Harbin Engineering University, Harbin, China, Post Code: 150001), GAO Jian-min, LU Hui-lin (College of Energy Science and Engineering, Harbin Institute of Technology, Harbin, China, Post Code: 150001) // Journal of Engineering for Thermal Energy & Power. — 2010, 25(6). —621~626

By simulating the particle phase flow based on the particle kinetic theory and taking into account the two phase interaction by using the fluid and particle two phase flow theory, established was a CFD (computational fluid dynamics) model featuring the multiple phase flow inside a fluidized bed nuclear reactor, and numerically simulated and studied were the fluid kinetic behaviors in the abovementioned reactor. The calculation results show that the distribution of particle concentrations on the cross section obtained by using Gidaspow drag force model shares a comparatively close tendency to that of the currently available test results. The particle concentration at the center of the central jet zone is relatively high. After dropping step by step to a partial minimum value, it will gradually increase with an increase of the radial distance. The particle concentration in the annulus zone remains basically unchanged. The influence of the action force between the fluid and particles as well as the particle elastic recovery coefficient etc. on the kinetic characteristics of the fluid in the reactor was analyzed. The research results show that the greater the particle collision recovery coefficient, the more uniform the particle concentration distribution on the cross section in the flow field. Key words: fluidized bed nuclear reactor, two-phase flow theory, numerical simulation

循环流化床锅炉热效率统计分析研究 = Statistical Analysis and Study of the Thermal Efficiencies of a Circulating Fluidized Bed Boiler[刊, 汉] / JIANG Shao-jian, LIU Le, AI Yuan-fang (College of Energy Science and Engineering, Central South University, Changsha, China, Post Code: 410083), HE Xiang-zhu (Hunan Provincial Energy Conservation Center, Changsha, China, Post Code: 410007) // Journal of Engineering for Thermal Energy & Power. — 2010, 25(6). — 627 ~ 629

In the light of the problem that the adoption of the empirical comparison method has a poor adaptability to the furnace volume of a CFB boiler, a power function regularity was used to perform a fitting of the operating data of a CFB boiler. On this basis, the relationship between the thermal efficiency and the main influencing factors (such as ton steam effective volume, volatile content of the coal) of the boiler was studied and a concept of ton steam effective volume put forward. The research results show that the tonnage steam effective volume and the volatile content of the coal burned are the major factors influencing the furnace type selection. To make the thermal efficiency of the boiler attain over 80%, the tonnage steam effective volume (represented by letter y) and the volatile content of the coal (represented by letter x) shall meet the requirement below: $y \geqslant 7.78x^{0.136}$. Key words: circulating fluidized bed boiler, furnace volume, volatile content, regression analysis, thermal efficiency, ton steam effective volume

炉内燃烧器射流组组合特性分析 = Analysis of the Jet Flow Group Combination Characteristics of an In-furnace Burner[刊, 汉] / SHI Guang-mei, LI Ming-hai, CHEN Jun, et al (Structural Mechanics Research Institute, Chinese Academy of Engineering Physics, Mianyang, China, Post Code: 621900) // Journal of Engineering for Thermal Energy & Power. — 2010, 25(6). — 630 ~ 634

With an oil-fired boiler serving as a concrete object of study, the in-furnace three-dimensional turbulent flow combustion field characteristics were numerically simulated by adjusting several main combination modes of the burners and the regularity of the jet flow group combination characteristics of the burners influencing the in-furnace aerodynamic field was obtained. A comparison of the simulation calculated results with the test ones shows that the calculated data are in relatively good agreement with the actually measured ones. This is of realistic significance for determining the combined operating condition of the burners and designing a test scheme, thereby providing a theoretical reference and basis for regulating the operating condition of in-door oil-fired boilers. Key words: turbulent flow combustion, jet flow group combination characteristics, numerical simulation, oil-fired boiler